SOLID-STATE MICROREFRIGERATION IN CONJONCTION WITH LIQUID COOLING

Younes Ezzahri and Ali Shakouri

Department of Electrical Engineering, University of California
Santa Cruz, California, USA, 95064
younes@soe.ucsc.edu & ali@soe.ucsc.edu

ABSTRACT

Thermal design requirements are mostly driven by the peak temperatures. Reducing or eliminating hot spots could alleviate the design requirement for the whole package. Combination of solid-state and liquid cooling will allow removal of both hot spots and background heating. In this paper, we analyze the performance of thin film Bi_2Te_3 microcooler and the 3D SiGe based microrefrigerator and optimize the maximum cooling and cooling power density in the presence of flow. Liquid flow and heat transfer coefficient will change the background temperature of the chip but they also affect the performance of the solid-state coolers used to remove hot spots. Both Peltier cooling at interfaces and Joule heating inside the device could be affected by the fluid flow. We analyze conventional Peltier coolers as well as 3D coolers. We study the impact of various parameters such as thermoelectric leg thickness, thermal interface resistances, and geometry factor on the overall system performance. We find that the cooling of conventional Peltier cooler is significantly reduced in the presence of fluid flow. On the other hand, 3D SiGe can be effective to remove high power density hot spots up to 500W/cm². 3D microrefrigerators can have a significant impact if the thermoelectric figure-of-merit, ZT, could reach 0.5 for a material grown on silicon substrate. It is interesting to note that there is an optimum microrefrigerator active region thickness that gives the maximum localized cooling. For liquid heat transfer coefficient between 5000 and 20000 W/m²/K, the optimum is found to be between 10 and 20 µm.

1. INTRODUCTION

Thermoelectric cooling is used for temperature stabilization and control of small area devices. Compared to the traditional heat pumps, thermoelectric coolers (TEC) have the advantages of compactness, high reliability, low maintenance, no vibration (because of no moving parts), no refrigerants, easy control and direct electric energy conversion. Thermoelectric coolers are currently used in microelectronic and optoelectronic applications. Because of their low efficiency, their use is limited to small powers or localized cooling.

Efforts have been made to develop a model that predicts the cooling performance of a TEC in a real application including the effect of the heat transfer coefficients at the cold and hot sides, as well as the effect of thermal contact resistance of ceramic plates and electrical contact resistances of metallic interconnects; very interesting and detailed theories can be found in these references [1-5]. In this paper, we expand the previous studies to the case where TECs are placed inside a microchannel with liquid flow.

The basic thermoelectric energy conversion is determined by the material's figure-of-merit ZT. ZT is defined by $ZT = \frac{\sigma S^2}{\beta} T$, where σ, S, and β are the electrical conductivity, Seebeck coefficient and thermal conductivity of the thermoelectric material respectively. SiGe is a well known bulk thermoelectric material for high temperature power generation applications. Recently, Si/SiGe superlattice structures have been investigated for room temperature cooling applications [2]. Si-based microrefrigerators are attractive for their potential monolithic integration with Si microelectronics.

Another advantage of thermoelectric devices is their ability to be combined with other conventional liquid cooling techniques [6], which can offer an additional degree of freedom to remove both background heating and hot spots. Hot spots have become one of the major problems in IC industry. Removing them has become one of the biggest challenges for the thermal management of the electronic and optoelectronic chips. Hot spots and non-uniform temperature distribution in the chip can degrade the performance and reduce the reliability. Unfortunately, most of the existing cooling techniques can not remove the hot spots selectively and they have to operate in a sub-optimal fashion and over-cool the whole chip [7]. To overcome these difficulties, one solution is to use hybrid solid-state and liquid cooling.

Two-phase flow is a well known technique that can provide a high cooling power density, but it has flow instabilities issues due to the creation and dynamics of gas

bubbles inside the microchannel. Integrating thermoelectric coolers will allow condensation of the bubbles and reduce such flow instabilities. Hybrid solid-state/liquid cooling is a promising technique to remove both the background heating and the hot spots.

In this paper we will analyze the cooling performance of a conventional thin film Bi_2Te_3 TEC and a 3D SiGe based microrefrigerator and optimize the maximum cooling and cooling power density in the presence of liquid flow. According to ref [7] spot cooling inside a microchannel can be used for bubble condensation and the control of the two-phase flow. In this application, it is important to study the maximum cooling and cooling power density of the solid-state cooler as a function of the flow parameters, heat transfer coefficient and the liquid temperature. We also study the impact of various parameters such as thermoelectric leg thickness, Ohmic electrical contact resistance, and ceramic thermal contact resistance, on the overall spot cooling performance.

2. THERMOELECTRIC MODEL

In this section, we present the theoretical modeling of the cooling performance of both a conventional thin film Bi_2Te_3 TEC and the 3D SiGe based microrefrigerator.

1.1 Conventional thin film TEC

Figure 1 illustrates a schematic diagram of a commercial TEC with heat exchangers at both the cold and hot sides. It consists of several n-p thermoelectric couples sandwiched between two electrically insulated but thermally conductive ceramic plates. It is assumed that the thermoelectric arms of the TEC, n-type and p-type, have symmetric structures and properties. Moreover we assumed all thermoelectric properties to be temperature independent and refer to the normal values of the commercially available Bi_2Te_3 thin film. The TEC is assumed to be well insulated from the surrounding except the heat flows at the cold and hot sides [4, 5].

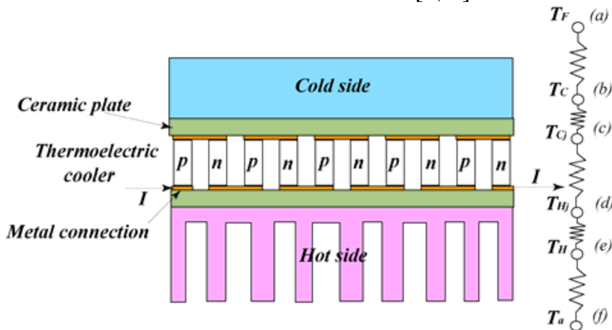

Figure 1: Schematic diagram of a thermoelectric cooler (TEC) and the corresponding thermal network model.

Application of the thermal network model to the TEC as shown in figure 1, allows us to obtain the heat balance equations from up to down at positions (a)-(f) as follows [4, 5]:

$$\begin{cases} Q_C = H_F A\left(T_F - T_C\right) \\ Q_C = K_C\left(T_C - T_{C_J}\right) \\ Q_C = I_e S T_{C_J} - \frac{1}{2} R I_e^2 - K\left(T_{H_J} - T_{C_J}\right) \\ Q_H = I_e S T_{H_J} + \frac{1}{2} R I_e^2 - K\left(T_{H_J} - T_{C_J}\right) \\ Q_H = K_C\left(T_{H_J} - T_H\right) \\ Q_H = H_H A\left(T_H - T_a\right) \end{cases} \quad (1)$$

where Q_C, Q_H are the cooling rate at the cold side and the heat rejection rate at the hot side, respectively. T_F and T_a are the temperatures of the heat source (fluid), and the heat sink (ambient); T_C, T_H, are the temperatures of the cold and hot sides; T_{CJ} and T_{HJ}, are the temperatures of the cold and hot junctions (i.e. the temperatures of the cold and hot metal electrodes). I_e is the electrical current. H_F and H_H are the overall heat transfer coefficients of the heat exchangers at the cold and hot sides. A is the surface area of the heat exchangers. K_C denotes the thermal conductance of the ceramic plate, which is supposed to be the same at the top and bottom of the TEC. It is given by:

$$K_C = \frac{\beta_C A}{t_C} \quad (2)$$

where β_C and t_C are the thermal conductivity and thickness of the ceramic plate, respectively.
S, R, and K are the total Seebeck coefficient, electrical resistance, and thermal conductance of the TEC, respectively. They are given by:

$$\begin{cases} S = \left(S_P - S_n\right) N = 2 S_{pn} N \\ R = \left(\frac{L_P}{\sigma_P A_P} + \frac{L_n}{\sigma_n A_n} + 2\frac{r_{oc}}{A_P} + 2\frac{r_{oc}}{A_n}\right) N = \left(2\frac{1}{\sigma_{pn} G} + 4\frac{r_{oc}}{A_{pn}}\right) N \\ K = \left(\beta_P \frac{A_P}{L_P} + \beta_n \frac{A_n}{L_n}\right) N = 2\beta_{Pn} G N \\ G = \frac{A_{pn}}{L_{pn}} \end{cases} \quad (3)$$

G is called the geometrical factor of the TEC, and N is the total number of the p-n thermoelectric couples. $A_p=A_n=A_{pn}$ is the cross section area of the TEC n-type and p-type legs, and $L_p=L_n=L_{pn}$ are their lengths. r_{oc} is the Ohmic electrical contact resistance at the interface metal/semiconductor, in which we can include also the electrical resistance of the metal electrode.
By eliminating T_{CJ} and T_{HJ} from the system of equations (1), the latter could be written as:

$$\begin{cases} Q_C = H_F A\left(T_F - T_C\right) \\ Q_C = I_e S_{eq}^C T_C - \frac{1}{2} R_{eq}^C I_e^2 - K_{eq}\left(T_H - T_C\right) \\ Q_H = I_e S_{eq}^H T_H + \frac{1}{2} R_{eq}^H I_e^2 - K_{eq}\left(T_H - T_C\right) \\ Q_H = H_H A\left(T_H - T_a\right) \end{cases} \quad (4)$$

where equivalent impedances have been introduced, $S_{eq}^{C}, S_{eq}^{H}, R_{eq}^{C}, R_{eq}^{H}$, and K_{eq} to include the effect of the thermal conductance of the ceramic plates and the electrical contact resistance of the metal electrodes. They are respectively given by:

$$\begin{cases} S_{eq}^{C}=S\dfrac{1-J_e}{1+2\kappa-J_e^2};\ S_{eq}^{H}=S\dfrac{1+J_e}{1+2\kappa-J_e^2} \\ R_{eq}^{C}=R\dfrac{1+2\kappa-J_e}{1+2\kappa-J_e^2};\ R_{eq}^{H}=R\dfrac{1+2\kappa+J_e}{1+2\kappa-J_e^2} \\ K_{eq}=\dfrac{K}{1+2\kappa-J_e^2} \\ J_e=\dfrac{I_e S}{K_C} \text{ and } \kappa=\dfrac{K}{K_C} \end{cases} \quad (5)$$

The second and third equations of system (4) resemble the ones of an ideal TEC except for the equivalent impedances. This procedure has been first introduced by X. C. Xuan [5]. Xuan gave the same equivalent Seebeck coefficient and electrical resistance felt by the cold and hot side of the TEC. However, we found that the cold and hot sides have slightly different expressions of the equivalent Seebeck coefficient and electrical resistance, but the equivalent thermal conductance is the same.

Solving the system of equations (4) is straightforward, from which we can get the expressions of different parameters T_C, T_H, Q_C, Q_H, as well as the expression of the *coefficient of Performance* $COP=\dfrac{Q_C}{Q_H-Q_C}$. The temperature at the cold side of the TEC is given by:

$$T_C=H_F A\frac{K_{eq}^{H}}{K_{eq}^{2}+K_{eq}^{C}\times K_{eq}^{H}}T_F-H_H A\frac{K_{eq}}{K_{eq}^{2}+K_{eq}^{C}\times K_{eq}^{H}}T_a +\frac{1}{2}\frac{R_{eq}^{C}\times K_{eq}^{H}-R_{eq}^{H}\times K_{eq}}{K_{eq}^{2}+K_{eq}^{C}\times K_{eq}^{H}}I_e^2 \quad (6)$$

In expression (6), two more equivalent thermal conductances have been introduced, namely K_{eq}^{C}, and K_{eq}^{H} which are given by:

$$\begin{cases} K_{eq}^{C}=I_e S_{eq}^{C}+K_{eq}+H_F A \\ K_{eq}^{H}=I_e S_{eq}^{H}-K_{eq}-H_H A \end{cases} \quad (7)$$

The *cooling power density (CPD)* of the TEC is defined as the needed thermal load to be put on the cold side to make the temperature at this location equals ambient temperature T_a. By combination of the two first equations of the system of equation (4), the *CPD* could easily be derived as:

$$CPD=I_e S_{eq}^{C}T_a-\frac{1}{2}R_{eq}^{C}I_e^2-K_{eq}\left(T_H-T_a\right) -H_F A\left(T_F-T_a\right) \quad (8)$$

1.2 3D microrefrigerator

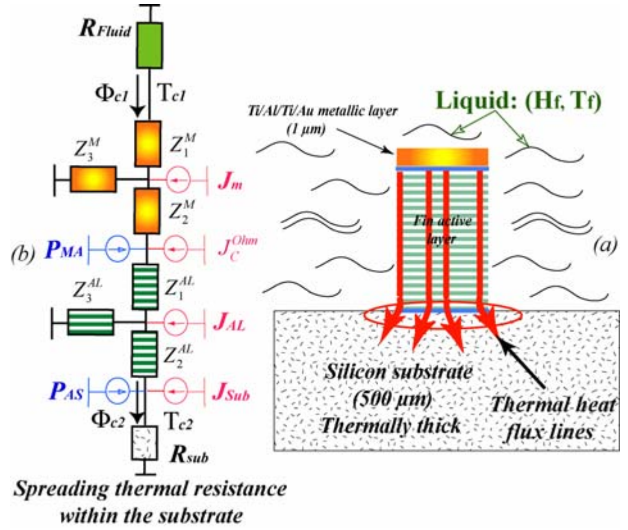

Figure 2: Schematic diagram of the 3D SiGe based microrefrigerator (a) and its corresponding thermal quadrupoles circuit (b).

Modeling of the cooling performance of the 3D SiGe microrefrigerator is based on Thermal Quadrupoles Method (TQM) [8-10]. The TQM is a general analytical model that can be used to calculate electrical and thermal responses in a 3D geometry and in the AC regime, thus making it possible to distinguish, in some cases, the Peltier effect from the Joule effect. In the case of a pure sine wave electrical excitation, the Peltier effect appears at the same frequency as the operating current, whereas the Joule effect appears at the double frequency. The precision of TQM allows its application in the detailed characterization of thermoelectric material properties [11]. This method has been used to model the behavior of a conventional thermoelectric couple (Bi_2Te_3) [12], and recently it has been applied to Si/SiGe microrefrigerator [13]. The model presented here uses the limit of the TQM at long times (i.e. steady-state behavior).

We consider a simple structure of the SiGe microrefrigerator as illustrated in figure 2.a. The device is made of a thin film SiGe active layer grown on top of a silicon substrate, and on top of which a metal layer is deposited. There is no cap layer and no buffer layer as different from former configurations [9, 10]. Also, to capture the intrinsic cooling performance of the SiGe microrefrigerator, we neglect all thermal leakages due to the top metal lead. Thermophysical properties of the microrefrigerator are assumed to be temperature independent.

In the modeling, the microrefrigerator top surface temperature variation is calculated by taking into account all possible mechanisms of heat generation and conduction within the entire device. 3D heat and current spreading in the substrate is taken into account using analytic formulas. A detailed description of TQM to model the steady state cooling performance of 3D SiGe

based microrefrigerators is presented in reference [10]. In the following we present the TQM modeling for the simple proposed SiGe microrefrigerator in presence of fluid flow.

Both the top metal layer and the active SiGe layer are several orders of magnitude larger than the mean free path of both electrons and phonons [14]. We can hence assume a diffusive transport regime, and the Fourier heat equation can then be used. When the active layer is a superlattice, because individual layers within it are very thin, on the order of nanometers, the superlattice is considered as an effective medium.

The thickness of the active SiGe layer is very small compared to that of the substrate; moreover, all Peltier sources are uniform at all junction plans. We thus consider the heat transfer across the microrefrigerator to be one-dimensional in the cross-plane direction of the device. Heat transfer at the side surface area around the mesa due to convection by the fluid is also taken into account. Our structure is formed of two essential layers; solving the heat equation using the fin approximation allows writing the heat transfer matrix of each layer in the form:

$$\begin{pmatrix} T_{in} \\ \phi_{in} \end{pmatrix} = \begin{pmatrix} A_i & B_i \\ C_i & D_i \end{pmatrix} \begin{pmatrix} T_{out} \\ \phi_{out} \end{pmatrix} - \begin{pmatrix} Z_1^i \\ 1 \end{pmatrix} J_i \qquad (9)$$

The matrix coefficients are respectively given by:

$$M_i = \begin{pmatrix} A_i & B_i \\ C_i & D_i \end{pmatrix} = \begin{pmatrix} ch(q_i t_i) & \dfrac{sh(q_i t_i)}{\beta_i q_i \Sigma} \\ \beta_i q_i \Sigma sh(q_i t_i) & ch(q_i t_i) \end{pmatrix} \qquad (10)$$

where: $q_i^2 = \dfrac{2H_F}{\beta_i r}$, r being the equivalent radius of the microrefrigerator and Σ is its cross section area $\Sigma = \pi r^2$. β_i is the thermal conductivity of layer i and t_i is its thickness. The heat transfer coefficient of the fluid is described by H_F.

Z_1 is one of the three thermal impedances by which the heat transfer within each layer can be represented (figure 2. (b)). These thermal impedances are function of the matrix coefficients, and they are given by:

$$Z_1^i = \frac{A_i - 1}{C_i} = Z_2^i \text{ and } Z_3^i = \frac{1}{C_i} \qquad (11)$$

The term J_i represents the internal Joule heating source inside each layer that takes the fluid flow into consideration, and is given by:

$$J_i = R_i^{ele} I_F^2 \frac{sh(q_i t_i)}{q_i t_i} \qquad (12)$$

R_i^{ele} is the electrical resistance of each layer, and I_F is the amplitude of an effective electrical current given by:

$$I_F^2 = I_e^2 + \frac{2\pi H_F t_i r}{R_i^{ele}} (T_F - T_a) \qquad (13)$$

T_F and T_a are the fluid and ambient temperatures, respectively.

The subscript i=M and AL, stands for the metallic layer and the active SiGe layer, respectively.

Regarding the local character of the microrefrigerator, the silicon substrate underneath it is considered thermally thick and its effect will be contained in what is called the *Resistance of constriction or spreading*. Constriction and spreading resistances exist whenever heat flows from one region to another of different cross-sectional area. The term constriction is used to describe the situation where heat flows out from a large cross-sectional region into a narrower one, and the term spreading is used to describe the opposite case where heat flows out of a narrow region into a larger cross-sectional area.

Approximating both the microrefrigerator and the substrate with a cylindrical geometry, it is easy to show that the thermal constriction/spreading resistance can be given by [8]:

$$R_{Sub}^{the} = \frac{8}{3\pi^2 \beta_{Sub} r}, \text{ with } r = \sqrt{\Sigma / \pi} \qquad (14)$$

where r is the radius of the contact disc between the two media, Σ is the cross-sectional area of the microrefrigerator, and β_{Sub} is the thermal conductivity of the substrate.

In fact, the expression of this constriction/spreading resistance depends on the form of temperature and heat flux distributions in the [0, r] interval. Equation (14) is valid in the case of uniform heat flux distribution in this interval which should match better the physics. One should note however, that the difference in the expressions of the constriction/spreading resistances between the case of uniform heat flux distribution and the case of uniform temperature distribution in the [0, r] interval is only 8% [8]. In addition to the thermal spreading inside the substrate, there is an electrical current spreading. This electrical spreading is characterized by a spreading of the electrical current density lines in the substrate. Heat current flow is different from electrical current flow due essentially to the notion of skin effect related to electrical current. However, this notion has no significance in the DC regime and the electrical constriction/spreading resistance can be calculated in analogy with the thermal resistance, and is given by the equation:

$$R_{Sub}^{ele} = \frac{8}{3\pi^2 \sigma_{Sub} r} \qquad (15)$$

where r is the radius of the contact disc between the microrefrigerator and the substrate, and σ_{Sub} is the electrical conductivity of the substrate.

We also demonstrated in previous works [9, 10] that the Ohmic contact resistance R_C^{Ohm} between the active layer and the metallic layer is another important limiting factor on the performance of the microrefrigerator.

Figures 2 (a) and 2 (b) illustrate respectively, a schematic diagram of the SiGe microrefrigerator surrounded by the fluid and its corresponding thermal quadrupoles circuit in the DC regime.

Application of Kirchhoff laws to this circuit, allows us to get a matrix relation, which represents the DC heat

transfer in the entire structure between $\begin{pmatrix} T_{C1} \\ \phi_{C1} \end{pmatrix}$ and $\begin{pmatrix} T_{C2} \\ \phi_{C2} \end{pmatrix}$, the temperature-heat flux vectors at the top metallic layer and the interface active layer/substrate, respectively:

$$\begin{pmatrix} T_{C1} \\ \phi_{C1} \end{pmatrix} = M_M M_{AL} \begin{pmatrix} T_{C2} \\ \phi_{C2} \end{pmatrix} - M_M M_{AL} \begin{pmatrix} 0 \\ P_{AS} \end{pmatrix}$$
$$-M_M \begin{pmatrix} Z_1^{AL} J_{AL} \\ J_{AL} + P_{MA} + J_C^{Ohm} \end{pmatrix} - \begin{pmatrix} Z_1^M J_M \\ J_M \end{pmatrix} \qquad (16)$$

where:

$$\begin{cases} P_{MA} = \left(S_M - S_{AL}\right) I_e T_0, \;\; P_{AS} = \left(S_{AL} - S_{Sub}\right) I_e T_0 \\ J_{Sub} = R_{Sub}^{ele} I_e^2, J_C^{Ohm} = R_C^{Ohm} I_e^2 \\ \phi_{C2} = \dfrac{T_{C2}}{R_{Sub}^{the}} - \dfrac{1}{2} J_{Sub} \end{cases} \qquad (17)$$

S_M, S_{AL}, and S_{Sub} are the absolute Seebeck coefficients of the metal layer, active SiGe layer, and substrate, respectively. The effective active layer Seebeck coefficient, S_{AL}, include both thermoelectric and thermionic contributions in the case where the active layer is a Si/SiGe superlattice. T_0 is the average temperature of the junction. Previous simulations in the general case of the AC regime have shown that for small excitation current amplitudes, linear approximation is still possible and approximating the interface temperature with the room temperature is still reasonably correct [10, 12]. For this reason, in the whole simulation, we keep the average temperature of the junction equal to the room temperature 300K [10, 12].

Combining Eqs. (16) and (17) allows us to get the expression of the microrefrigerator top surface temperature variation T_{C1} as function of the excitation current amplitude I_e, as well as all physical and geometrical parameters of the whole device. The expression of the T_{C1} is given by:

$$T_{C1} = \frac{1}{G_{Tot}} \begin{Bmatrix} \left(AD - BC\right)\left(P_{AS} + \dfrac{1}{2} J_{Sub}\right) + \\ \left[\left(AD_m - B_m C\right) + \dfrac{BD_m - B_m D}{R_{Sub}^{the}}\right]\left(P_{MA} + J_C^{Ohm}\right) \\ + \left(A + \dfrac{B}{R_{Sub}^{the}}\right)\left(\Delta + Q_F + Q_H\right) - \left(C + \dfrac{D}{R_{Sub}^{the}}\right)\Gamma \end{Bmatrix} (18)$$

G_{Tot}, Q_F, Δ, and Γ are defined by:

$$\begin{cases} G_{Tot} = \Sigma H_F \left(A + \dfrac{B}{R_{Sub}^{the}}\right) + C + \dfrac{D}{R_{Sub}^{the}} \\ Q_F = \Sigma H_F \left(T_F - T_a\right) \\ \Delta = \left(C Z_1^{AL} + D\right) J_{AL} + J_M \\ \Gamma = \left(A Z_1^{AL} + B\right) J_{AL} + Z_1^M J_M \end{cases} \qquad (19)$$

where A, B, C, and D represent the coefficients of the matrix product $M_M M_{AL}$.

Q_H describes the thermal load at the top surface of the microrefrigerator. In our case, Q_H is supposed to be the power density of a hot spot or what is needed to condense a bubble.

The cooling power density CPD of the microrefrigerator top surface is defined by the thermal load that has to be put on this surface to make the temperature variation T_{C1} equals zero. According to this definition, we found the following expression for the CPD of the 3D microrefrigerator:

$$CPD = \frac{1}{\left(A + \dfrac{B}{R_{Sub}^{the}}\right)} \times$$
$$\begin{Bmatrix} \left(BC - AD\right)\left(P_{AS} + \dfrac{1}{2} J_{Sub}\right) + \\ \left[\left(B_m C - AD_m\right) + \dfrac{B_m D - BD_m}{R_{Sub}^{the}}\right]\left(P_{MA} + J_C^{Ohm}\right) \\ + \left(C + \dfrac{D}{R_{Sub}^{the}}\right)\Gamma - \left(A + \dfrac{B}{R_{Sub}^{the}}\right)\left(\Delta + Q_F + Q_H\right) \end{Bmatrix} (20)$$

3. RESULTS AND DISCUSSION

We start our discussion by first analyzing the temperature variation of both the 3D SiGe based microrefrigerator and the conventional Bi_2Te_3 thin film TEC. Figures 3 (a) and 3 (b) respectively show these behaviors.

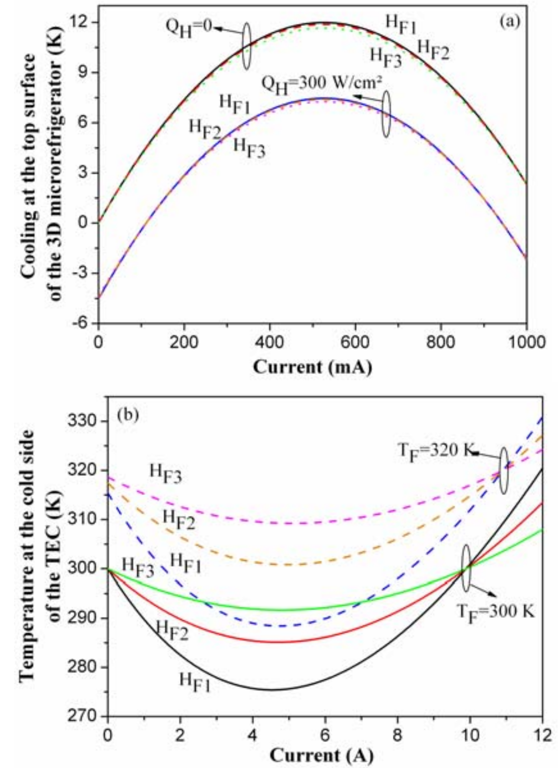

Figure 3: Temperature variation at the cold side of the 3D SiGe based microrefrigerator (a) and the conventional Bi_2Te_3 thin film TEC (b).

In these figures and all coming figures H_{F1}, H_{F2}, H_{F3} refer to *5000 W/m²/K*, *10000 W/m²/K* and *20000 W/m²/K*, respectively. In the case of the conventional TEC, the heat exchanger at the hot side is supposed to have a high value of heat transfer coefficient of $H_H=10^5$ *W/m²/K*. This value is kept constant for all simulation results. Tables 1 and 2 recapitulate the parameter values used for the simulation results given in the paper for both the 3D microrefrigerator, and the conventional TEC, respectively.

Table 1: Physical and geometrical properties used for the simulation of the 3D SiGe based microrefrigerator cooling performance. The microrefrigerator size is *50x50 µm²*, and the *ZT* of the active layer is *ZT=0.1*. The electrical contact resistance at the interface Metal layer/Active layer was assumed to be $r_{oc}=10^{-7}$ Ωcm^2.

Layer	Metal	Active SiGe layer	Substrate
S (µV/K)	8	235	445
σ ($\Omega^{-1}.m^{-1}$)	150/T_a//LN	3.65×10^4	3.1×10^4
β (W/m/K)	150	6	130
t (µm)	1	8	500 Thermally and Electrically thick

Table 2: Physical and geometrical properties used for the simulation of the conventional Bi_2Te_3 thin film TEC cooling performance. t_C is the thickness of the AlN ceramic plates at both the top and the bottom of the device. β_C is the bulk thermal conductivity of AlN. The electrical contact resistance at the interface Metal layer/Active layer was assumed to be $r_{oc}=0$ Ωcm^2.

Parameter	value	parameter	value
A (mm²)	9.6×9.6	$\beta_p=\beta_n=\beta_{pn}$ (W/m/K)	1.45
$A_p=A_n=A_{pn}$ (mm²)	0.16	$\sigma_p=\sigma_n=\sigma_{pn}$ ($\Omega^{-1}.m^{-1}$)	1.065×10^5
$L_p=L_n=L_{pn}$ (µm)	0.2	$S_p=-S_n=S_{pn}$ (µV/K)	200
t_C (µm)	0.25	β_C (W/m/K)*	285
N		60	

As we can see in figures 3, the effect of the fluid heat transfer at the cold side of the conventional TEC is obvious, for the same temperature of the fluid, the minimum temperature at the cold side of the TEC increases by increasing the heat transfer coefficient H_F. The same behavior is observed when H_F is fixed and we increase the fluid temperature T_F.
On the other hand, the minimum temperature at the cold side (maximum cooling) of the 3D microrefrigerator is not very sensitive to the variation of H_F for a fixed value of the thermal load Q_H. This makes the 3D microrefrigerator more attractive than the conventional thin film TEC to be used in the hybrid solid-state/liquid cooling techniques.

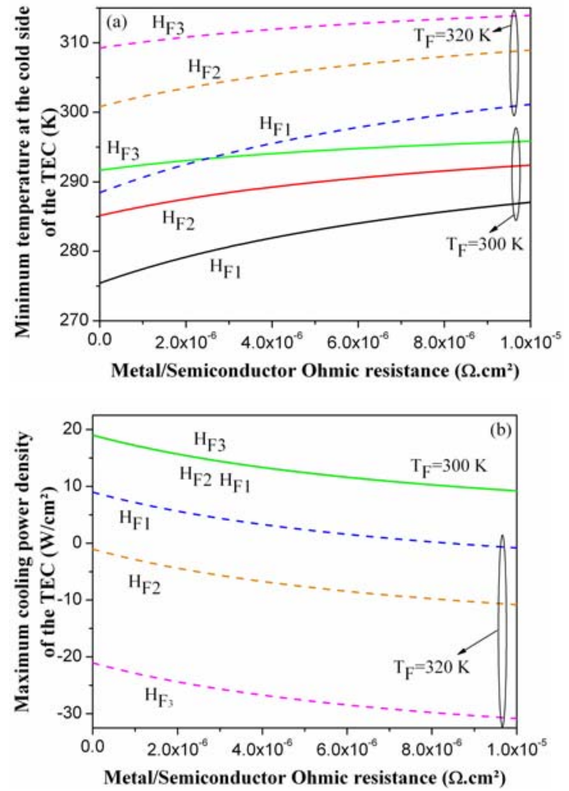

Figure 4: Variation of the minimum T_C (a) and the maximum *CPD* (b) of the conventional TEC as a function of r_{oc}.

In figures 4, are reported the behaviors of the minimum temperature T_C and the maximum *CPD* of the conventional BiTe TEC as a function of the Ohmic electrical contact resistance at the interface Metal/Semiconductor (a) and (b). To generate these curves the rest of the properties of the TEC are kept constant, (Table 2). As it is seen in figures 4 (a) and (b), increasing the Ohmic contact resistance, increases the minimum T_C and reduces the maximum *CPD* since it causes an additional Joule heating source. We can also see that the effect of this electrical interface resistance diminishes by increasing the value of H_F. Increasing H_F degrades more the cooling performance of the TEC.
On the other hand, both the minimum T_C and the maximum *CPD* are not sensitive to the variation of the thermal conductance of the ceramic plate when we changed its thickness from *100 µm* to *650 µm*. Changing the ceramic plate thermal conductance from 50-250W/K does not affect the cooling power density and the minimum cold side temperature.
Also we can see in figure 4 (b) that the maximum *CPD* is not sensitive to the value of H_F when the temperature of the heat exchanger at the cold side (fluid in our case) is taken equal to the ambient temperature ($T_F=T_a=300K$). The negative values of the *CPD*, means that the TEC stops cooling because of the large thermal load introduced by the high value of the fluid temperature T_F and/or its heat transfer coefficient H_F.

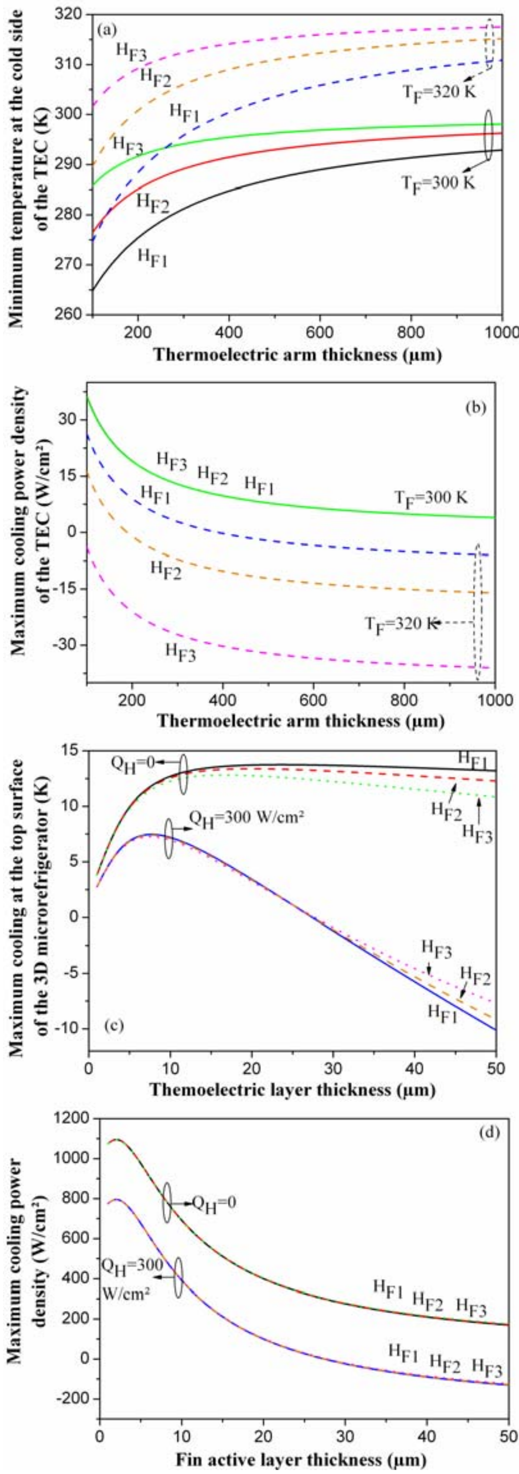

Figure 5: Variation of the maximum cooling and the maximum *CPD* for the conventional TEC (a) and (b) and the 3D microrefrigerator (c) and (d) as a function of the thermoelectric layer thickness.

Figures 5 (a) and (b) show the variation of the maximum cooling (difference between the minimum temperature at the cold side and ambient temperature), and the maximum *CPD* of the conventional Bi_2Te_3 thin film TEC as a function of the thickness of the thermoelectric arms L_{pn}. As expected, by decreasing L_{pn}, both the maximum cooling and the maximum *CPD* increase. It is noteworthy to mention that by decreasing the length of the thermoelectric arms L_{pn}, the optimum current increases. Thus the effect of the electrical contact resistances starts to be more significant, and Joule heating due to these resistances starts to compete with Peltier cooling at the interfaces. As a consequence of this interplay, an optimum L_{pn} is generally found, for which the cooling performance of the conventional TEC reaches its maximum. We have not considered the effect of electrical contact resistances in our simulation of the TEC and the value of r_{oc} was kept $r_{oc}=0$.

In figures 5 (c) and (d) are reported the variation of the maximum cooling and the maximum *CPD* of the 3D SiGe microrefrigerator as a function of the thermoelectric layer thickness. It is interesting to note the existence of an optimum thickness that gives the best cooling performance of the device. The value of the optimum thickness decreases by increasing the thermal load Q_H and/or the fluid heat transfer coefficient H_F. We can see also from figure 5 (d), that the *CPD* for a fixed Q_H is almost insensitive to the variation of H_F.

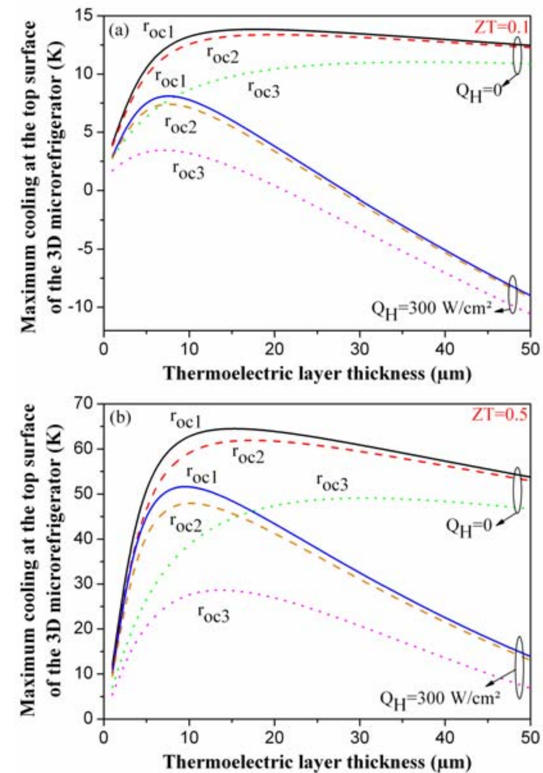

Figure 6: Variation of the maximum cooling of the 3D SiGe microrefrigerator as a function of the thermoelectric layer thickness for *ZT=0.1* (a) and *ZT=0.5* (b) of the active thermoelectric layer. H_F is fixed to 10^4 W/m²/K.

To check out how the optimum thickness of the thermoelectric layer is sensitive to other parameters of the 3D microrefrigerator, we have done further simulations by changing the value of r_{oc} at the interface Metal/Active layer and the value of the ZT of the active thermoelectric layer. The results of these simulations are reported in figures 6 and 7.

Figures 6 (a) and (b) show the variation of the maximum cooling of the 3D SiGe microrefrigerator as a function of the thermoelectric layer thickness for two different values of the figure of merit of the active thermoelectric layer $ZT=0.1$, and $ZT=0.5$. Three different values of r_{oc} have been taken in this simulation $r_{oc1}=0$, $r_{oc2}=10^{-7}$ $\Omega.cm^2$ and $r_{oc3}=10^{-6}$ $\Omega.cm^2$. As we can see in the figures, the position of the optimum thickness depends in a complicated way on the values of ZT, r_{oc}, and Q_H. More particularly, increasing ZT increases the maximum cooling as it is expected, but shifts up or down the position of the optimum thickness depending on the value of Q_H. Here we assume ZT of the active layer is increased by decreasing its thermal conductivity.

On the other hand, increasing r_{oc} seems to shift up this position, and lower the maximum cooling.

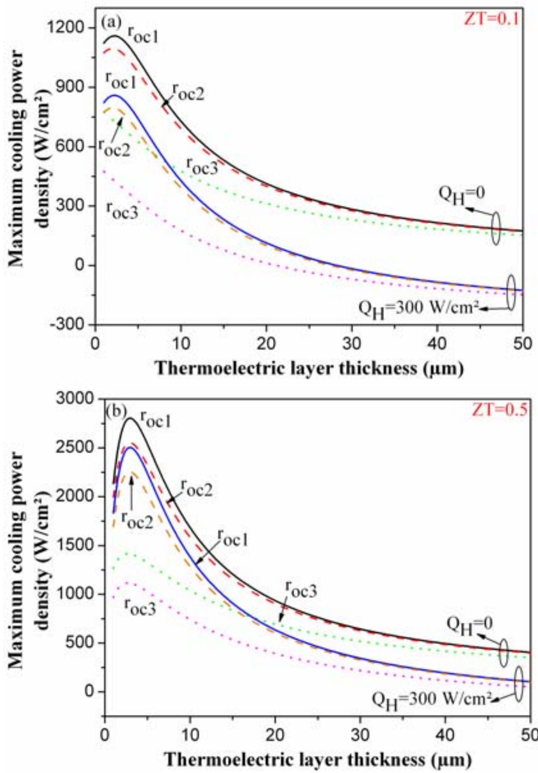

Figure 7: Variation of the maximum *CPD* of the 3D SiGe microrefrigerator as a function of the thermoelectric layer thickness for *ZT =0.1* (a) and *ZT= 0.5* (b) of the active thermoelectric layer. H_F is fixed to 10^4 $W/m^2/K$.

The variation of the maximum *CPD* of the 3D SiGe microrefrigerator as a function of the thermoelectric layer thickness is reported in figures 7 (a) and (b) for the same two different values of $ZT=0.1$, and $ZT=0.5$, and the same three different values of r_{oc}. In this case increasing r_{oc} seems to shift down slightly the position of the optimum thermoelectric layer thickness for the maximum *CPD*.

The effect of the thermal load Q_H on the position of the optimum thickness of the thermoelectric layer is reported in figures 8 for both the maximum cooling (a) and the maximum *CPD* (b) of the 3D microrefrigerator. Three different values of Q_H are considered in combination with two different values of the ZT of the active thermoelectric layer as has been assumed in figures 6 and 7. The values of Q_H considered are $Q_H=0$, $Q_H=300$ W/cm^2 and $Q_H=700$ W/cm^2.

As we can see in figures 8, increasing Q_H shift down the value of the optimum thickness of the active thermoelectric layer for the maximum cooling. On the other hand, we see also that the cooling capacity of the 3D microrefrigerator can still be effective even with a thermal load of *700 W/cm²* with a maximum cooling approaching *3K* and a maximum CPD approaching 400 W/cm² for an active SiGe thermoelectric layer of $ZT=0.1$.

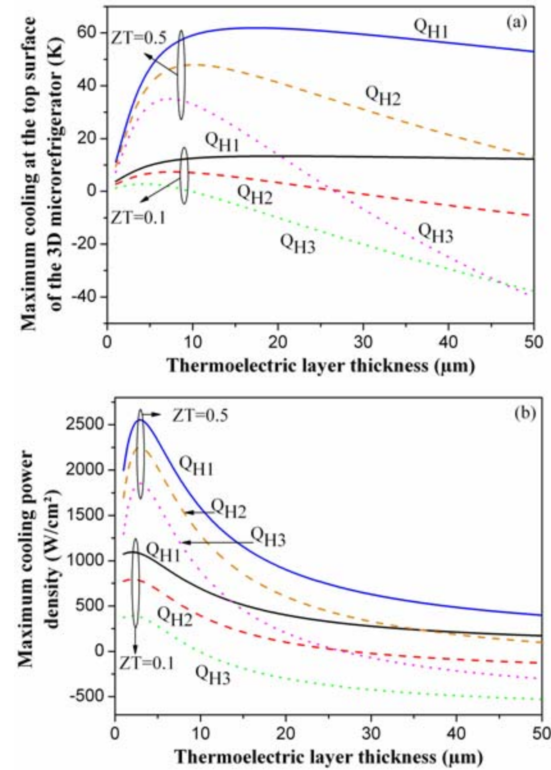

Figure 8: Variation of the maximum cooling (a) and the maximum *CPD* (b) of the 3D microrefrigerator as a function of the thermoelectric layer thickness for different values of *ZT* and the thermal load Q_H. H_F and r_{oc} are fixed to 10^4 $W/m^2/K$ and 10^{-7} Ωcm^2, respectively.

4. SUMMARY

We have presented in this paper a comparison of the cooling performances of the 3D SiGe based microrefrigerator and a conventional Bi_2Te_3 thin film TEC in the presence of fluid flow. The motivation of this work was to study the effect of the fluid temperature T_F and the heat transfer coefficient H_F on the cooling performance of the thermoelectric devices. The study has shown that the cooling performance of the 3D SiGe microrefrigerator is less affected by the variation of either T_F or H_F. On the other hand, the cooling performance of the conventional TEC depends highly on the values of these parameters. Furthermore, the impact of the geometry of the thermoelectric devices on their cooling performances has also been presented. *3D microrefrigerators can have a significant impact if the thermoelectric figure-of-merit, ZT, could reach 0.5 for a material grown on silicon substrate.* The small size of the 3D microrefrigerator and its high cooling values make it the potential candidate to be integrated into microchannel in which it can be used to condensate bubbles and thus improve the performance of two-phase flow cooling systems.

5. ACKNOWLEDGEMENTS

The authors would like to acknowledge the support of the Interconnect Focus Center, one of the five research centers funded under the Focus Center Research Program, a DARPA and Semiconductor Research Corporation program.

6. REFERENCES

[1] H. J. Goldsmid, 1986, "*Electronic refrigeration*", London, Pion.

[2] D. M. Rowe, 1995, "*Handbook of Thermoelectrics*", CRC.

[3] M. Yamanashi, 1996, "A new approach to optimum design in thermoelectric cooling systems" *Journal of Applied. Physics*. **80**, 5494-5502.

[4] X. C. Xuan, 2002, "Optimum design of a thermoelectric device", *Semiconductor Science and Technology*, **17**, 114-119.

[5] X. C. Xuan, 2003, "Investigation of thermal contact effect on thermoelectric coolers", *Energy Conversion and Managment*, **44**, 399-410.

[6] A. B. Cohen, M. Arik, and M. Ohadi, 2006, "Direct liquid cooling of high flux micro and nano electronic components", *Proceeding of the IEEE*, **94**, 1549-1570.

[7] V. Sahu, Y. Joshi, and A. Federov, 2008, "Hybrid solid-state/Fluidic cooling for hot spot removal", *Proceeding of the ITherm 2008*.

[8] D. Maillet, S. André, J. C. Batsale, A. Degiovanni, and C. Moyne, 2000, *THERMAL QUADRUPOLES: Solving the Heat Equation through Integral Transforms*, John Wiley & Sons.

[9] Y. Ezzahri, S. Dilhaire, L. D. Patino-Lopez, S. Grauby, W. Claeys, Z. Bian, Y. Zhang, and A. Shakouri, 2007, "Dynamical behavior and cut-off frequency of Si/SiGe microcoolers", *Superlattices and Microstructures*, **41**, 7-16.

[10] Y. Ezzahri, G. Zeng, K. Fukutani, Z. Bian, and A. Shakouri, 2008, "A comparison of thin film microrefrigerators based on Si/SiGe superlattice and bulk SiGe", *Microelectronics Journal*, **39**, 981.

[11] L. D. Patino-Lopez, S. Grauby, Y. Ezzahri, W. Cleays, and S. Dilhaire, 2006, "Harmonic regime analysis and inverse methods applied to the simultaneous determination of thermoelectric properties", *Proceeding of the 25rd International Conference on Thermoelectrics*, Vienna, Austria, August 6-10.

[12] L. D. Patiño-Lopez, 2004, PhD Thesis, ON 2792, University Bordeaux 1, France.

[13] Y. Ezzahri, 2005, "Etude du Transport des Phonons dans les Microréfrigérateurs à base de Super-réseaux Si/SiGe", PhD Thesis, ON 3090, University Bordeaux 1, France.

[14] J. M. Ziman, 1960, "*Electrons and Phonons*", C. Press, Oxford.